ELSEVIER

Journal of Molecular Catalysis A: Chemical 115 (1997) 431–448

JOURNAL OF MOLECULAR CATALYSIS A: CHEMICAL

Modelling of structure, sorption, synthesis and reactivity in catalytic systems [1]

C.R.A. Catlow *, L. Ackermann, R.G. Bell, D.H. Gay, S. Holt, D.W. Lewis, M.A. Nygren, G. Sastre, D.C. Sayle, P.E. Sinclair

The Royal Institution of Great Britain, 21 Albemarle Street, London W1X 4BS, UK

Abstract

We illustrate the current status of the application of computer modelling methods to catalytic systems by taking recent examples from modelling of both long range and local structural properties of microporous materials, surface structures of oxides, sorption in zeolites, host–template interactions in aluminophosphates and reaction mechanisms on oxide surfaces and at acid sites in zeolites. We emphasise the role of modelling techniques in the interpretation of experimental studies in catalysis.

1. Introduction

Computer modelling techniques have been extensively and increasingly applied in recent years to the study of structure and reactivity in catalytic materials. As described in several recent articles [1–3] they can make vital and unique contributions to the following fundamental problems in catalytic science:

(1) Development of models of the structures at the atomic level of crystalline and amorphous catalysts, including both bulk and surface structures.

(2) Elucidation of the structure of *local* states which provide the active sites in solids or on their surfaces.

(3) Determination of the mechanisms of molecular diffusion to and docking at active sites.

(4) Understanding of detailed reaction mechanisms of docked molecules at active sites.

Such information is, of course, essential in the development of a molecular understanding of catalysis. Molecular modelling has therefore a central role to play in contemporary catalytic studies.

Modelling of catalysts makes use of the full range of currently available atomistic simulation techniques. These comprise both 'forcefield' (or interatomic potential based) methods and electronic structure techniques. The former include energy minimisation (EM), Monte Carlo (MC) and molecular dynamics (MD) techniques; while the latter embrace both Hartree–Fock (HF) and density function theory (DFT) methodologies which may be applied to clusters or periodic

* Corresponding author.

[1] Communication presented at the First Francqui Colloquium, Brussels, 19–20 February 1996.

PII S1381-1169(96)00349-4

arrays of atoms. In the case of cluster calculations, it is highly desirable, whenever possible, to include an approximate representation of the embedding matrix provided by the surrounding lattice.

Details of currently available methods and their implementation are available in several recent reviews [4,5]. We also note that the development of the field has been assisted by the availability of high quality, general purpose computer codes, and that contemporary molecular graphics provides an essential tool for the analysis and interpretation of the results of computer modelling studies.

Broadly speaking, forcefield methods are most appropriately applied to modelling structures, docking and diffusion, although key configurations may be refined by electronic structure techniques; electronic structure methods are, of course, essential in modelling reaction mechanisms. As will be shown later in this paper and in the articles of van Santen [6] and Norskov [7], modelling methods are moving in the direction of increasingly accurate prediction of systems of growing complexity.

In the sections which follow we describe recent applications from our laboratory which demonstrate both the accuracy and increasingly predictive character of modelling studies in this field. The synergy between computational and experimental techniques is also emphasised.

2. Applications

We now highlight recent work that illustrates the range and diversity of contemporary modelling studies in catalysis.

2.1. Modelling structures

Knowledge of the structure of catalysts at the atomic level is of course the first prerequisite for a molecular understanding of catalysis. Possibly the most challenging problems are posed by the structure of microporous materials. We now review three recent applications in the field. The first concerns a subtle problem in the crystallographic (long range) structure of an important material; the other two relate to key local structural properties of direct importance to catalysis.

2.1.1. Structural features of $AlPO_4$-5

Microporous framework materials such as aluminosilicates (zeolites) and aluminophosphates (AlPOs) are, typically, microcrystalline. Therefore, unlike many other heterogeneous catalysts, their structure often cannot be examined routinely using single crystal diffraction techniques. High resolution powder diffraction now allows us to solve complex structures. Nevertheless, detailed and important aspects of the structures may be obscured in the crystallographic refinement of these systems. An important and topical example concerns T–O–T angles (where T=Si or Al in zeolites and Al or P in AlPOs). Such angles typically take values between 140–165° [8]. However, certain published structures exhibit almost linear (176–179°) angles [9,10]. We have recently investigated this effect in $AlPO_4$-5 [11].

We performed lattice energy minimisation calculations on a variety of unit cell models of $AlPO_4$-5 using the pair potential model of Gale and Henson [12]. We investigated not only the previously published structure [10] (hexagonal *P6cc* spacegroup) but also a more recent structure (orthorhombic *Pcc2*) obtained using a combination of X-ray and neutron data [13]. We further constructed supercells of the hexagonal structure.

We find that it is not possible to optimise fully the structure of $AlPO_4$-5 in the *P6cc* spacegroup, as indicated in our calculation by the inability to locate an energy minimum. This result had previously been noted by other workers [14,15]. However, if we reduce the symmetry to a *P6* spacegroup (Table 1), then an energy minimum configuration can be obtained (as also found by Henson et al. [15]). This reduction in symmetry removes constraints im-

posed by the *P6cc* spacegroup on the linear Al–O–P angles and allows these angles to take up more typical values. The effect was further confirmed by calculations on supercells of the hexagonal *P6cc* cell. Only when the symmetry was lowered in such a way as to allow optimisation of the linear Al–O–P angle did we find an energy minimum. We found that the orthorhombic cell [13], which does not contain any such linear angles, is also a minimum energy configuration, albeit slightly higher in energy than the *P6* unit cell, by 0.5 kJ mol^{-1} per unit cell. Given that entropic effects are not included in these calculations, we conclude that interconversion between structures with these two spacegroups would be likely.

If we consider the structure of the material in terms of angles and bond lengths (Table 1, Fig. 1) it is clear that the structures are very similar, and that it is the selection of the spacegroup in the structure solution which makes them different. Furthermore, our results have more general implications regarding the structure solution of such materials. We have seen that the imposition of a high symmetry spacegroup has resulted in anomalous bond angles and bond lengths. Although refinement of the complex structure and microcrystalline nature of these materials often dictates that high symmetries are used, we conclude that refinements which exhibit such anomalous structural features would benefit from re-refinement in a lower symmetry spacegroup. Clearly from this and other examples [9,16,17] computational methods can prove of great value in obtaining accurate structures for such complex materials.

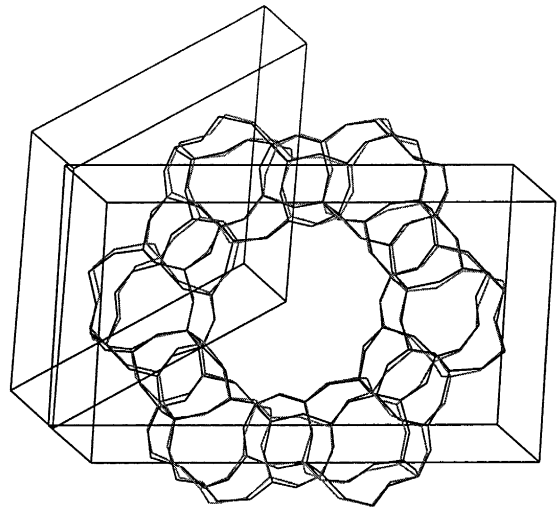

Fig. 1. Overlay of the calculated minimum energy structures of $AlPO_4$-5 in both *P6* (dotted lines) and *Pcc2* spacegroups.

2.1.2. Modelling Si distribution in SAPO-5

Our next example concerns possibly the most important local structural property of microporous aluminophosphates, where it is known that introduction of framework substituting ele-

Table 1
Structural parameters for various unit cell models for $AlPO_4$-5

Structure	Experimental *P6cc* [10]	Simulated *P6cc* [a]	Simulated *P6*	Experimental *Pcc2* [13]	Simulated *Pcc2*
$E_{lattice}$ (eV per $AlPO_4$)	—	−268.0408	−268.0643	—	−268.0587
(a) (Å)	13.771	13.820	13.759	13.797	13.754
(b) (Å)	13.771	14.138	13.759	23.899	23.900
(c) (Å)	8.379	8.678	8.393	8.417	8.417
α (°)	90.0	90.0	90.0	90.0	90.0
β (°)	90.0	90.0	90.0	90.0	90.0
γ (°)	120.0	120.0	120.0	90.0	90.4
Al–O (Å)	1.68–1.73	1.696–1.722	1.712–1.734	1.67–1.76	1.693–1.731
P–O (Å)	1.46–1.53	1.507–1.523	1.505–1.530	1.44–1.56	1.504–1.528
(Al–O–P) (°)	149–178	147.6–176.4	141.8–154.7	147–156	140.1–156.5

[a] Note this structure is not an energy minimum, but rather a transition state as negative phonon modes are present in lattice dynamical calculations on the structure.

ments in AlPO structures often results in the generation of materials with high catalytic activity in processes requiring medium-high acid strength [18]. For example, when silicon is introduced into a neutral $AlPO_4$ framework, Brønsted acid sites are created, resulting in materials which can be exploited as catalysts. These silico–alumino–phosphates (SAPOs) are effective for the conversion of light olefins to gasoline, catalytic reforming of naphthenes, and for the isomerisation of C_8 aromatics [19]. However there are many questions regarding the mechanism of Si incorporation and their distribution in the framework. For example, it is known that Si can aggregate forming Si islands at certain concentrations, although such behaviour differs in different SAPO structures [20]. We have recently used simulation methods to investigate these effects and now present results pertaining to SAPO-5 [21].

Silicon can be incorporated into an AlPO via two substitution mechanisms:

AlPO framework	SAPO framework
SM2:	
$[AlPO_4] + Si^{4+} + H^+ \rightarrow$	$[Si,H]_P + P^{5+}$
SM3:	
$[AlPO_4] + 2Si^{4+} \rightarrow$	$[2Si]_{Al,P} + P^{5+} + Al^{3+}$

The notation used shows the species present in the final (in square brackets) and the initial structures (in subscripts). We note that these formal processes are components of a Born–Haber cycle: other reactions are needed as sources of 'Si^{4+}' and sinks of 'P^{5+}' and 'Al^{3+}'. The structure of the species is illustrated schematically in Fig. 2.

We initially investigated the structural deformations resulting from Si substitution by the mechanism of Brønsted site formation (SM2). These deformations were found only to affect the structure as far as the first neighbouring T site from the substituent, suggesting that long range effects are small and that there may be little difference in Si substitution energy via this mechanism in any other AlPO structure. However, the structural changes at the site where the substitution takes place are quite significant, the resulting bond lengths and angles being summarised below:

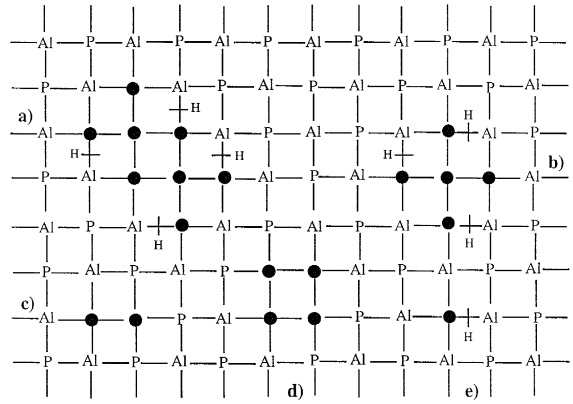

Fig. 2. Different Si aggregates produced in SAPO-5 (● ≡ Si). (a) $[8Si,4H]_{2aL,6P}$; (b) $[5Si,3H]_{Al,4P}$; (c) $[2Si]_{Al,P}$; (d) $[4Si]_{Al,2P}$; (e) $[Si,H]_P$.

	T–O(Å)	O–Al(Å)	TOAl(°)
$AlPO_4$-5 (T = P)	1.52	1.72	149.0
SAPO-5 (T = Si)	1.78	1.82	136.9

We then consider the interactions of two Brønsted sites in SAPO-5. Two different conformations were modelled with a varying topological distance between the two acid sites. We find that a configuration of the type –Si–Al–P–Al–Si– has an energy of ≈ 0.17eV lower than that in which two Si substituents are infinitely separated, hence revealing a tendency for the Si to cluster. These findings are in agreement with ^{29}Si NMR measurements [22] in which, at low Si content, a single peak corresponding to Si(4Al)(12P) is observed. As the Si content increases, signals corresponding to Si with some Si in the second or first T environment start to appear. It is also observed that when the Si content in SAPO-5 is $> 10\%$ of the T atoms, signals corresponding to Si(0Al) appear [23], corresponding to the presence of Si islands [23]; we have therefore performed calculations on such structures.

Many possible Si islands can be simulated in any given SAPO structure depending on the amount of Si atoms present and the topology of its distribution. It appears that even when the silicon content is not very high in SAPO-5, small Si islands are formed. We have therefore determined the stability of islands containing 4, 5, and 8 Si atoms. The stability of these islands has been tested in terms of their relative energy with respect to smaller (more dispersed) aggregates. The calculations gave the following results:

Process	Energy (eV)
4Si island:	
$[4Si]_{2Al,2P} \rightarrow 2[2Si]_{Al,P}$	+0.68
5Si island:	
$[5Si,3H]_{Al,4P} \rightarrow [2Si]_{Al,P} + 3[Si,H]_{P}$	+0.46
8Si island:	
$[8Si,4H]_{2Al,6P} \rightarrow [4Si]_{2Al,2P} + 4[Si,H]_{P}$	+1.23

The conformations for all the aggregates shown in the equations are again schematised in Fig. 2. The 4Si island is generated by two substitutions described in SM2, while the 5Si and 8Si islands are obtained by means of a combination of SM2 and SM3 substitution. We find that a 4Si island is more stable than two 2Si islands, which can be rationalised in terms of the number of [Si–O–P] linkages present in each of the conformations. Fig. 2 shows 4[Si–O–P] linkages in the 4Si islands and 6[Si–O–P] linkages in the two 2Si islands. The instability created by these linkages is in part due to the high electrostatic repulsion generated by the proximity of tetra and pentavalent cations. The absence of [Si–O–P] linkages in SAPO structures has been experimentally established [25] and these calculations provide an energetic rationalisation of this effect. The 5Si island is also found to be more stable than a 2Si island and three Brønsted acid sites. Again, the result can be explained in terms of the number of [Si–O–P] linkages. The calculation on the 8Si island confirms not only the higher stability of an aggregate without [Si–O–P] linkages but also its higher stability with respect to a 4Si island. We can therefore conclude that Si island formation via a combination of SM2 and SM3 processes is the likely mechanism of substitution, a conclusion which is, once more, supported by experimental evidence [24].

2.1.3. Identification of the active site in the NO decomposition catalyst Cu-ZSM-5

The decomposition of NO by Cu-ZSM-5 has stimulated considerable interest in cation exchanged zeolite systems particularly with respect to their potential as vehicle exhaust catalysts [26] a focal point of which is to identify the active site which effects the catalysis.

To identify the active site in Cu-ZSM-5 we have constructed model systems based on the active catalyst preparation of Iwamoto et al. [27] with 96 silicon T-sites per unit cell. The experimental Si/Al ratio of 12 was effected by replacing, at random, 8 of the 96 silicon atoms with aluminium and the 150% copper loading achieved by introducing 4 Cu^{+} and $4Cu^{2+}$ ions at random extra-framework sites within the host zeolite with the excess charge compensated for by $4OH^{-}$ species. A simple computer program was written to construct 2000 ‘trial structures’ where the aluminium, copper and hydroxyl species were introduced at various random positions and the energy of each system calculated, with a full energy minimisation applied to the 20 systems with the lowest unrelaxed energy. The procedure should generate all low energy extra-framework copper configurations.

Analysis of the resulting copper clusters from the 20 fully relaxed systems revealed that 41% of the copper species were paired with the most common cluster being a hydroxyl-bridged Cu(I)–Cu(II) copper pair. The high occurrence of such species suggests that this structure is particularly stable and we suggest therefore that the cluster represents a good model for the active site. To refine further this particular structure, 1000[Cu(I)–OH–Cu(II)] species were

Table 2
Bond distances and coordination number (CN) of the active site within the Cu-ZSM-5 system

	Cu–O (Å)	Cu–OH (Å)	Cu–Cu (Å)	Cu–Al (Å)	CN
Cu(II)	2.00, 2.20, 2.29	1.69	3.10	1.89	4
Cu(I)	2.05, 2.10	1.91		3.24	3

introduced at random into ZSM-5 with a full energy minimisation performed on the 10 lowest energy configurations. The resulting, fully relaxed, lowest energy configuration is illustrated in Fig. 3 and Table 2. The figure clearly illustrates both the detailed configuration and location of the cluster within the ZSM-5 zeolite and we suggest is a useful model of the active site within the Cu-ZSM-5 NO decomposition catalyst. We also note the cluster is strongly bound to the host zeolite via a framework aluminium.

2.2. Modelling of surfaces: α-Fe_2O_3 surfaces

To understand how a catalyst functions at the atomistic scale, we need to understand the interface between the catalyst and reactants, intermediates and products. This requires a detailed knowledge of the surface structure of the catalyst. Here we focus on the modelling of hematite (α-Fe_2O_3), an oxidation catalyst. Its structure is the same as that of Corundum (α-Al_2O_3), but the morphology and chemical properties are quite different.

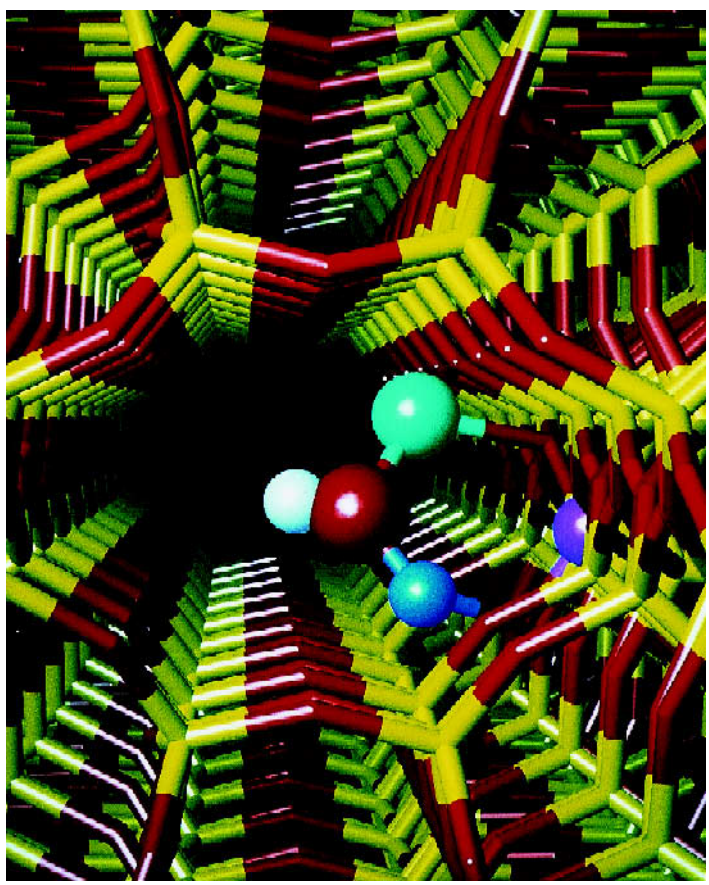

Fig. 3. Illustration of the refined active site structure and location in the Cu–ZSM–5 NO decomposition catalyst. Silicon is coloured yellow, lattice oxygen is red, hydroxyl oxygen is orange, hydrogen is white, aluminium is purple, Cu(II) are the small blue balls and Cu(I) the large blue balls.

The corundum structure can be described as a hexagonal close packed oxygen anion array with cations in the octahedral sites. In the case of Fe_2O_3 and Al_2O_3 the cations are too large to fit into the octahedral cavities without causing distortion.

The surfaces of hematite are usually covered with a layer of Fe_3O_4, a spinel structure. This certainly affects the chemical properties, but also introduces added complexity for the modeler, and thus the discussion of modelling this new surface will be left for a future publication. This present discussion is concerned with modelling the surface structure and crystal morphology of a purely corundum structured material.

Two different programs were used to develop the models of the surfaces: first GULP [28] (a lattice energy simulation code) to generate the fully equilibrated bulk structure. It is essential that the bulk structure be relaxed, otherwise residual strains will distort the surface structures. The relaxed bulk structure is used as input for MARVIN [29] which models the surfaces. The key features of MARVIN are that the energy is calculated as a 2D infinite lattice summation, with the electrostatic contributions being com-

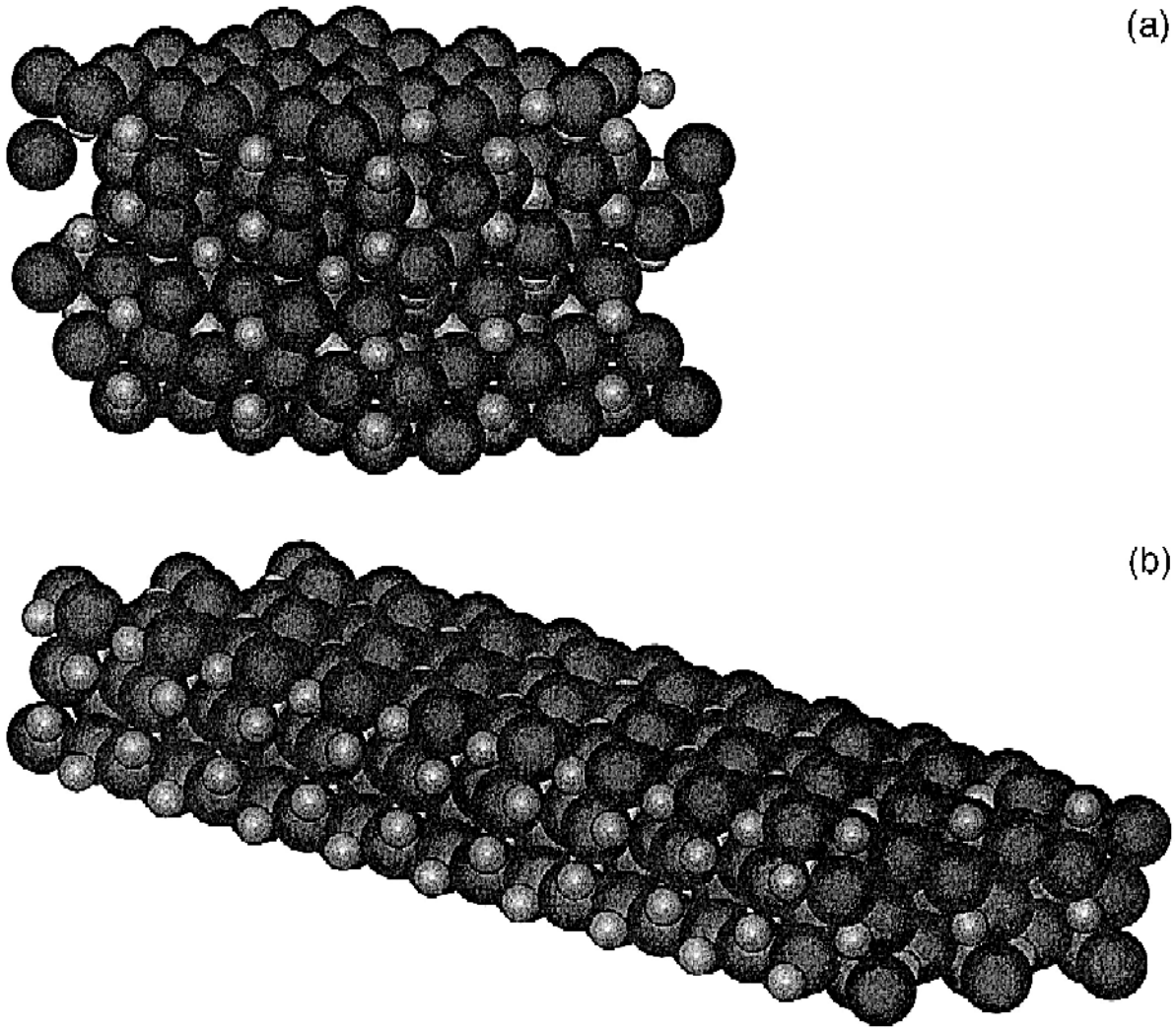

Fig. 4. Surface structure of (0001) (a) and the $(10\bar{1}2)$ (b) faces of hematite. Small spheres are metal cations; large spheres are oxygen anions.

puted using a 2D Ewald sum. This approach is more general than embedding 2D slabs in a 3D array. We note that MARVIN has been used successfully to model a wide variety of crystal types, including Al_2O_3 and Zircon [29], molecular/ionic crystals like $BaSO_4$ [30,31] and molecular crystals such as urea [32].

The surface structures shown in Fig. 4 illustrate two of the most stable faces. Their relative stability was determined by the calculated relaxed surface energy and attachment energy. The cleavage plane was selected so that there was no bulk dipole. Fig. 4 shows the availability of the different surface sites on the face. The detailed atomistic structure is of great value for understanding catalysis and adsorption processes.

The observed morphology of hematite (a hexagonal structure), are rhombohedral crystals with the basal plane (0001) and the $(10\bar{1}1)$ face being the dominant faces, although the growth conditions can have considerable effects on the final crystal shape. Predicting the morphology can be quite complex since real crystals are seldom of the same quality as theoretical ones. The prediction of crystal morphology is an essential starting point for surface modelling. The morphology provides a good technique for selecting which crystal faces are going to be important for the problems of interest, which could include adsorption, growth modification, defect segregation and catalysis.

Here we present two predicted morphologies (see Fig. 5). The equilibrium morphology is the morphology that gives the lowest energy for a given volume, and the crystal face with the lowest surface energy will be the dominant face exposed. The growth morphology is based on the attachment energy, which uses a simple kinetic approach to crystal growth. A crystal will grow in the direction of the highest attachment energy face with the largest (most negative) attachment energy thereby creating the adjacent faces. The morphology will be dominated by the slowest growing face, which will have the lowest (least negative) attachment energy.

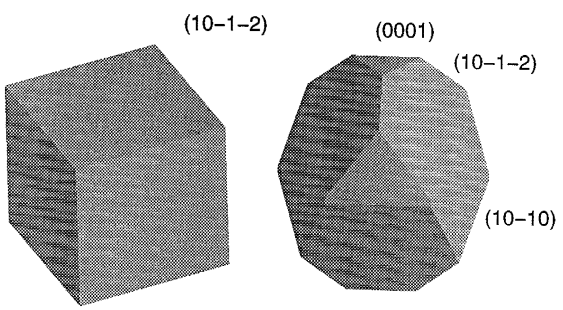

Fig. 5. Predicted growth and equilibrium morphologies of hematite.

Table 3
Surface and attachment energies for α-Fe_2O_3, before and after energy minimisation

Miller indices	Surface energy (J/m^2)		Attachment energy (eV)	
	before relaxation	after relaxation	before relaxation	after relaxation
(0001)	5.4	0.8	−107.31	−127.31
$(10\bar{1}4)$	6.0	1.0	−88.24	−107.28
$(10\bar{1}\bar{2})$	2.0	0.5	−20.24	−21.92
$(10\bar{1}\bar{8})$	6.4	1.9	−221.94	−240.670
$(10\bar{1}1)$	4.2	1.2	−96.03	−64.47
$(2\bar{1}\bar{1}0)$	3.0	0.8	−44.09	−40.76
$(10\bar{1}0)$	4.9	0.6	−185.60	−160.77
$(10\bar{1}2)$	6.4	1.1	−256.55	−362.69

From Table 3, we can see that energy minimisation (relaxation) plays an important role in the properties used to predict morphologies. Due to the way that surface energies are computed, which is as the difference between the energy of the simulation cell at the surface and the bulk, the surface energy will always decrease during energy minimisation. The same is not true of attachment energies. During minimisation, energy can be exchanged between the growth slice and interplanar interactions, yielding an attachment energy that can either increase of decrease. These two approaches will in general give different predicted morphologies.

In the case of hematite, we get two very different morphologies as shown in Fig. 5. Experimentally the (0001) and $(10\bar{1}1)$ faces domi-

Table 4
Inter-ionic layer (Å) spacing of the α-Fe_2O_3 (0001) face.

	Clean surface		Hydroxylated surface		
	unrelaxed	relaxed	unrelaxed	relaxed	
Fe–O	0.838	0.042	0.825	0.759	H–O
O–Fe	0.838	0.986	0.886	1.074	O–Fe
Fe–Fe	0.584	0.282	0.595	0.441	Fe–Fe
Fe–O	0.838	1.046	0.833	0.868	Fe–O
O–Fe	0.838	0.906	0.833	0.796	O–Fe
Fe–Fe	0.584	0.550	0.595	0.653	Fe–Fe
Fe–O	0.838	0.859	0.833	0.797	Fe–O
O–Fe	0.838	0.817	0.833	0.828	O–Fe

nate. From the calculated surface energies, we get the following ordering of morphological importance:

$$(10\bar{1}\bar{2}) > (10\bar{1}0) > (0001) > (2\bar{1}\bar{1}0) > (10\bar{1}4),$$

whilst using attachment energies, the ordering is:

$$(10\bar{1}\bar{2}) > (2\bar{1}\bar{1}0) > (10\bar{1}1) > (10\bar{1}4) > (0001).$$

Neither of these explain the observed crystal morphology. However, as mentioned previously, with hematite the surface is usually covered with layers of Fe_3O_4. Similarly, many metal oxide surfaces are covered with a hydroxide layer, which can change the relative morphological importance of the crystal faces. It would be of interest to investigate whether different morphologies closer to those predicted would be observed under growth conditions under which such surface layers are not formed. Future calculations will also test whether hydroxylated or non-stoichiometric surfaces generate crystal morphologies that are closer to those that are observed.

During the minimisation of the basal plane, the surface layers collapse (see Table 4), an effect previously noticed with the corundum structure. For corundum, the effect has been repeated with both classical potential models and quantum mechanical calculations. Recent work [33], has shown that a hydroxyl layer reduces this collapse and the resultant surface is more stable than the bare surface. This is also the case for hematite and we estimate the heat of reaction for water removal to be in the range of 5–8 eV. The structure of the relaxed surface (shown in Fig. 6) demonstrates a key feature of a hydroxyl termination of a surface, which is the complete covering of the metal ions. The presence of such hydroxyl groups will certainly have a considerable effect on the catalytic properties of the surface.

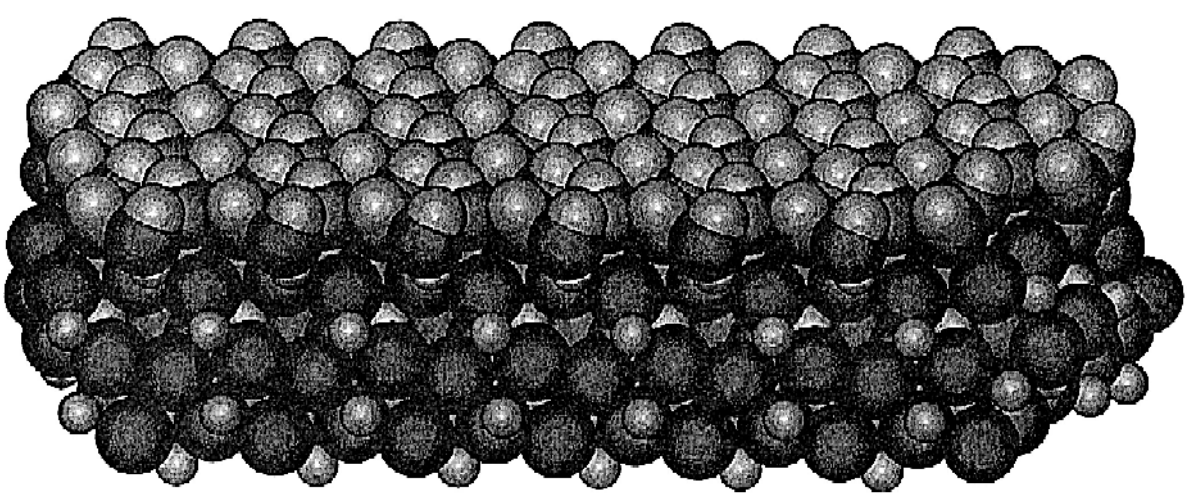

Fig. 6. Hydroxylated (0001) surface of hematite.

The calculations described in this section clearly show the critical role of the surface chemistry in influencing the morphology of oxide materials.

2.3. Modelling of sorption

Studying the locations and properties of organic adsorbates, such as catalytic reactants and template molecules, within the internal pores of zeolites poses a number of problems for the experimental scientist. Disorder, both static and dynamic, of the molecules is often encountered. Moreover the lighter elements of which organic molecules are composed, compared to aluminosilicate frameworks, make their detection by X-ray diffraction methods difficult although neutron diffraction techniques have succeeded in several systems in identifying the positions of sorbed molecules.

Probing the sorption sites of organic molecules using molecular modelling methods has provided an increasingly important adjunct to experimental methods. Both molecular dynamics (MD) and Monte Carlo methodologies, often in combination with energy minimisation, have been used successfully in this regard. In particular the automated Monte Carlo docking procedure of Freeman et al. [34], which blends all three methods, has proved especially suitable for locating minimum energy sites in zeolites channel systems. In the procedure, MD is first applied to the guest molecule, as though it were in the gas phase, in order to generate a library of conformations. Each of these conformations is then 'docked' into the zeolite framework using a Monte Carlo algorithm. The most favourable site/conformation combinations may subsequently be refined by energy minimisation to yield the overall minimum energy configuration.

Freeman and co-authors [34] originally deployed their automated docking procedure to study the sorption of isomers of butene in silicalite. Other key applications have involved butene in DAF-1 [35], butanols in ZSM-5 [36] and the modelling of template molecules in a range of zeolites [37–39]. Kaszkur and coworkers [40] have also demonstrated how molecular dynamics can be combined with powder X-ray diffraction, in a study of 1,4-dibromobutane in zeolite Y. In this work MD trajectories were obtained for the guest molecules and used to interpret synchrotron powder diffraction data recorded at two different temperatures. The simulations revealed that, at low temperatures, the dibromobutane is sorbed at a position spanning two of the framework supercages, with each Br atom located close to a Na^+ cation. At higher temperatures, one terminal Br remains sorbed while the other exhibits considerable thermal motion.

Recent work by Kaszkur and colleagues [41] used the Monte Carlo docking method to determine the position of *para*-xylene in ferrierite, a medium-pore zeolite which has found wide application as an acid catalyst. Rietveld refinement of high-resolution powder diffraction data, both X-ray and neutron, was complicated by considerable displacements to the framework atoms, observed after the *p*-xylene had been loaded into the sample. This suggested a violation of the *Immm* symmetry of the bare framework. Nevertheless it was possible to obtain a fit within this space group, albeit with large anisotropic temperature factors, the possibility of using lower symmetry models having been discounted due to the excessive numbers of independent parameters. In the light of these problems with symmetry, the accuracy of the *p*-xylene position, as determined from Fourier maps, might justifiably have been regarded with some reservation. Monte Carlo docking calculations were then carried out to attempt to confirm the location of the sorbate. The simulations used a $1 \times 1 \times 3$ supercell of the ferrierite framework, in order to exclude unrealistic molecule–molecule interactions, and involved full energy minimisation of both the framework and guest molecule.

The predicted minimum energy location of the molecule was in remarkable agreement with

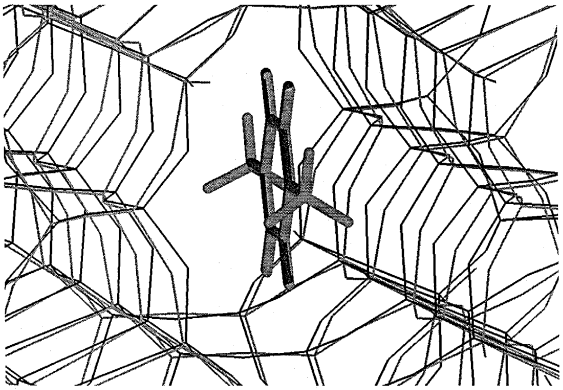

Fig. 7. Comparison between the experimental (black) and calculated (grey) sites for *p*-xylene in ferrierite. Methyl hydrogens are omitted from the experimental structure, since their positions are not uniquely defined.

that obtained experimentally (see Fig. 7) thus vindicating the approach taken in refining the diffraction data.

2.4. Simulation and synthesis: The competitive formation of $CoAlPO_4$-5 and $CoAlPO_4$-34 and the role of the template

Recent work, both computational [35,37,42–44] and experimental [45,46] has considered the role of templates in the formation of microporous materials. Much work has concentrated on elucidating how the shape of the template influences the product formed [42,43,45]. Our recent work [47] has expanded on these approaches by considering also the effects of the relative concentrations of both the metal cation (being introduced into the framework) and the template, and any co-operative effect they have in forming particular phases.

It is well documented that a cobalt–aluminophosphate gel containing triethylamine as a template can form either Co-$AlPO_4$-5 (AFI) or the chabazite (CHA) phase $CoAlPO_4$-34 [48–50]. The $CoAlPO_4$-5 phase is typically formed at higher temperatures and low Co concentrations, whilst high Co and template concentrations and lower temperatures favour the $CoAlPO_4$-34 structure. Furthermore, the CHA phase appears as an intermediate phase in certain gel compositions. We have therefore investigated how the template concentration and structure in these two materials can be influenced by the presence of heteroatoms in the gel and resulting crystalline material.

By performing calculations at different template concentrations we show how it is the combination of metal uptake, template–metal interaction and high template concentration which makes the formation of the $CoAlPO_4$-34 structure viable. We see (Table 5) that the interaction energy of the template with the framework does not increase markedly with increasing template concentration in the case of the AFI ($CoAlPO_4$-5) structure. We therefore expect that $CoAlPO_4$-5 formation is relatively insensitive to template concentration. However in CHA, there is a dramatic increase in the interaction energy with template concentration. We therefore propose, that high triethylamine concentrations are essential to stabilise the CHA phase. Consequently, assuming a direct correlation, under synthesis conditions, between the cationic triethylammonium template and the Co content (needed for electroneutrality of the bulk structure), a Co concentration equivalent to a

Table 5
Binding energies of triethylamine in the CHA and AFI structures. $E_{inter} = E_{host} - E_{free}$, where E_{host} is the total energy of the framework/template combination, E_{free} is the energy of an isolated gas phase template molecule. The results are normalised to give a E_{inter} per template. Similar trends are observed for triethylammonium. Note that these calculations are performed in siliceous analogues of the $CoAlPO_4$ systems

	Template concentration (per unit cell)	T site/template	E_{inter}/template (kJ mol^{-1})	
			no charges	with charges
CHA				
triethylamine	1	12	−47.3	−71.6
triethylamine	2	6	−61.1	−83.7
AFI				
triethylamine	0.25	48	−32.7	−62.7
triethylamine	0.5	24	−35.4	−64.1
triethylamine	1.0	12	−37.0	−66.8

bulk composition of $Co_{0.25}Al_{0.75}PO_4$ is required. We note that $CoAlPO_4$-34 usually forms with such a high Co concentration [48–50]. Furthermore, we note that AlPO-34 has not been reported, further supporting our hypothesis that interaction with anionic framework fragments are required to modify the gel in such a way as to make the formation of the CHA structure viable. Similar arguments limit the Co concentration in $CoAlPO_4$-5 to a composition of $Co_{0.17}Al_{0.83}PO_4$. Again, we note that $CoAlPO_4$-5 forms with Co concentrations of typically < 0.1 mol fraction. The inability to attain high purity $CoAlPO_4$-5 with high Co concentrations has been attributed to the formation of the $CoAlPO_4$-34 phase [48], a conclusion supported by these calculations. We would expect that, even at lower Co and template concentrations, the CHA phase can form, due to local concentration effects, but only as a transient and intermediate phase, thus disrupting the formation of phase pure $CoAlPO_4$-5 with an uniform Co concentration; a similar conclusion is drawn from diffuse reflectance spectroscopy [49]. Although the Co-template interactions have not been modelled directly, these calculations allow us to understand their role in the competitive formation of the two microporous structures. These interactions compel the templates to be present in concentrations appropriate for the formation of the CHA framework; without them the template packing is less dense resulting in the AFI structure. We consider that this effect is a general one as similar competitive behaviour is also noted with for example, SAPO-5/SAPO-34, SAPO-5/SAPO-44, $CoAlPO_4$-5/$CoAlPO_4$-35 and EU-1/EU-2, which we believe can all be explained by the interaction of framework cations with the template.

2.5. Reaction mechanisms

2.5.1. CH-bond activation on catalytic oxides

Oxidative coupling of methane (OCM) is known to be catalysed by a variety of oxidic materials [51]. Among these, Li/MgO (lithium doped magnesium oxide) may serve as the prototype. It has attracted a considerable number of investigations, both experimental [51,52] and theoretical [53–59] over the past decades. But although these studies created a large amount of data, many questions concerning the detailed nature of the physical and chemical processes involved are still to be clarified.

The catalytic activation of the process leading from methane to methyl radicals ($\cdot CH_3$, observed experimentally [60,61]) probably involves some kind of surface defect site. Evidence from e.p.r. measurements indicates a correlation between catalytic activity and the presence of O^- surface species [62,63]. In particular, the $[Li]^0$ centre has been proposed as an active site for OCM catalysis on Li/MgO [52]. The importance of this type of defect, consisting of an electron hole localised on an oxygen ion and stabilised by an adjacent Li (dopant) ion, has been demonstrated [64], but has also recently been questioned by the work of Lunsford and coworkers [52]. In several theoretical approaches $[Li]^0$ has served as a model of the active surface site [53–59]. Other defects known to be present on MgO surfaces (like dislocations and charged or neutral vacancies) may also be considered (see e.g. Refs. [58,65–67]).

Theoretical modelling of reactions at defective MgO surfaces has been undertaken by several workers employing different methods (ranging from EHT to MCSCF) [53–59,65–67]. More than 20 years ago, ab initio calculations were used to investigate H_2 bond breaking at a cation vacancy site [65] and computational studies of the role of MgO surface defects in catalysis have continued to be performed [67–69].

The main challenge lies in choosing an appropriate description of both (a) the surface defect and (b) the reaction. While (a) can be achieved through atomistic modelling (see e.g. Ref. [70]), (b) requires a quantum mechanical approach. As will be shown in the present work, however, the level of theory can affect results even qualitatively.

Since the long-range nature of the Madelung

field demands an accurate treatment, to satisfy (a) one has to go beyond the simplest (i.e. most localised) approximation. This can be done by using large cluster models (allowing substrate relaxation), embedding of some kind or a (pseudo) two-dimensional representation of the system (slab). Ideally a model should fulfil both (a) and (b) as well as possible, but unfortunately the prohibitively high computational cost involved still restricts the degree to which this goal may be reached. The present work is primarily concerned with (b); the transfer to larger, more realistic models (including surface relaxation) is reported elsewhere [71].

The process here envisaged, $CH_4 + [Li^+O^-]_s \rightarrow \cdot CH_3 + [Li^+(OH)^-]_s$ (index s indicates surface species) involves the homolytic breaking of a CH bond; in the same process an OH bond is formed. We note that open shell systems are present in both reactants and products. Therefore, an electronic structure calculation (and subsequent geometry optimisation) ought to be carried out at a sufficiently high level of theory. Starting from Hartree Fock (HF) SCF level this also includes taking into account electron correlation to some extent. Although computationally demanding, a way to do this systematically is by applying post-HF schemes (like MP2, MP4, etc.). Alternatively, and at much lower cost, one can use an approach based upon gradient corrected density functional theory (DFT). Recent improvements in the gradient corrections applied (in this work we use the B-LYP correction [72,73]) have rendered this method very well capable of determining geometries and energies with a high accuracy [74,75]. It seems therefore to be ideally suited for the requirements outlined above.

In previous studies [54,56] very simple models have been used to describe the interaction of methane with a $[Li]^0$ centre. An efficient, though still crude way of improving the quality of the model is by using a cluster embedded in an array of point charges. In our model (Fig. 8) only lithium, oxygen and methane are treated explicitly; the MgO crystal is represented by

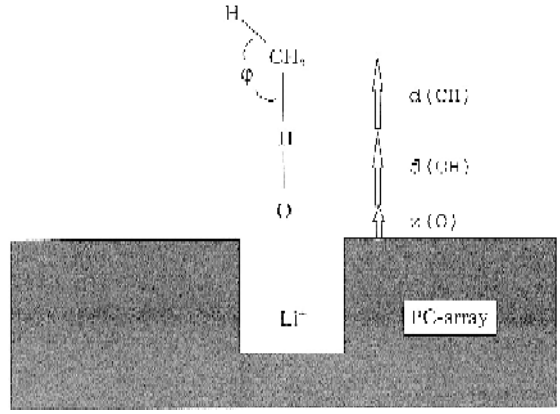

Fig. 8. The $[Li^+O^-]$–H–CH_3 model system. Its geometry is determined by the bond distances d(CH) and d(OH), the position of oxygen relative to the surface z(O) and the HCH angle. Li is kept fixed at 2.11 Å below the surface.

about 200 point charges ($q = \pm 2.0$ e) at their bulk positions. The CH and OH distances are varied and for each combination of d(CH) and d(OH) the remaining parameters are optimised. This is important for two reasons: (1) the oxygen ion accepting the hydrogen moves during this transfer process by several tenths of an Ångstrøm and (2) the methyl radical generated in the process tends towards a planar structure gaining an energy of about 0.3 eV.

The resulting energy surfaces (Fig. 9) display several important features and some significant differences. From HF-calculations (Fig. 9a) we find the classic shape of reactants valley (R), transition state (TS) and product valley (P). In contrast to the results of Zicovich–Wilson et al., however, this is not a late TS [54]; the saddle point is found in a rather symmetric position (at about 0.8 eV above the reactants level). This may be caused by the fact that the planarisation accompanying the release of $\cdot CH_3$ is only very crudely taken into account in Ref. [54]; their model differs from the one used in this study in the position the dopant atom assumes, but this is not likely to be the cause of such a pronounced, qualitative effect; furthermore, in omitting the ionic crystal field entirely, their description differs from the present one considerably.

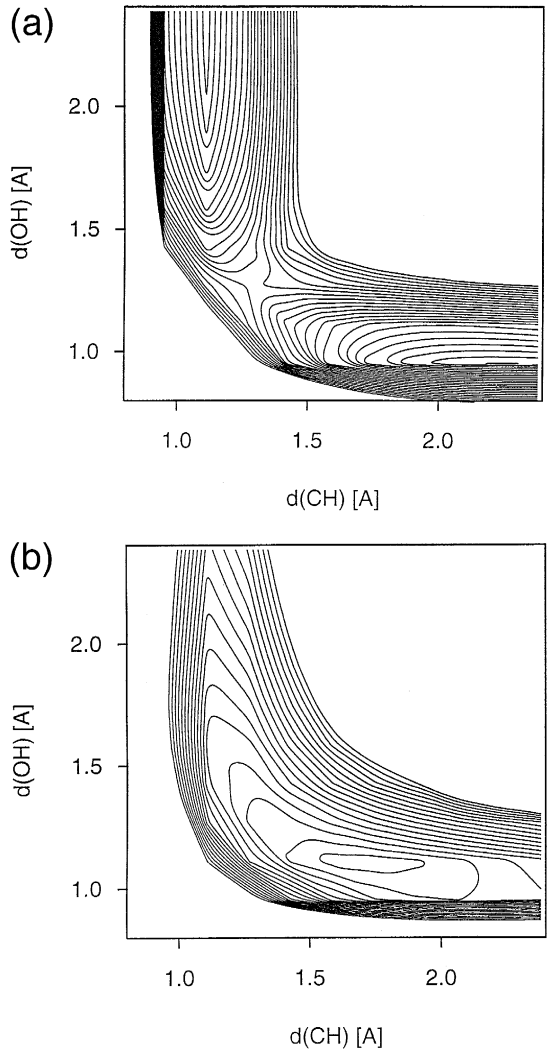

Fig. 9. The total energy of $[Li^+ O^-]$–H–CH_3 as a function of the CH and OH distance calculated using (a) HF and (b) B-LYP-DFT. The contour lines are spaced at 54 meV.

The surface resulting from B-LYP-DFT calculations is depicted in Fig. 9b. Here no TS is observed. In fact, the transition of hydrogen from carbon to oxygen occurs without activation barrier. However, some energy is needed for the release of the methyl radical fragment. The minimum found at a CH distance of 1.7 Å lies 0.43 eV below the product level (this value is reduced by a factor of two, when substrate relaxation is included [71]). Another difference seen in comparing Fig. 9a, b is a slightly shorter OH distance at the large d(CH) observed in the HF results. This may be a compensation effect for a slightly smaller z(O) in the DFT calculation, a (very moderate) overbinding effect.

The results presented here clearly demonstrate, that a complete neglect of electron correlation (pure HF) leads to a qualitatively different description of the methane dissociation process than is achieved by using an advanced (gradient corrected) DFT scheme. Thus, in further studies employing large clusters it will be essential to use methods that include electron correlation. Considering the computational cost involved, DFT appears to be ideally suited for this challenge.

2.5.2. Reactivity of methanol at alumino–silicate Brønsted acid site

In response to developments of fast computer technology and efficient computer algorithms, computational chemists are now able to probe the very complex nature of organic reactivity at heterogeneous surfaces. Of particular interest has been the prototypical methanol-to-gasoline (MTG) reaction [76] which, even after 20 years of experimental study (and more recently theoretical study), is still poorly understood.

Some years ago, Hutchings and Hunter suggested a mechanism for the MTG process in acidic zeolites that satisfied all of the accumulated experimental data [77]. They were also able to show that a number of popular mechanisms suggested in the literature were unlikely.

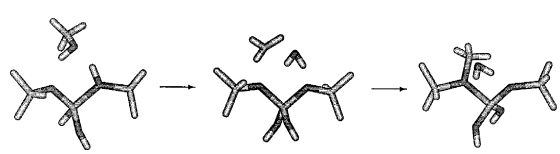

Fig. 10. TZVP/DFT(BLYP) optimised structures for the methylation of a model Brønsted acid site by one methanol molecule. The acid site is modelled by a $H_3SiOAl(OH)_2O(H)SiH_3$ cluster and the central structure is the transition state.

Their mechanism, the methyl oxonium ion mechanism, proceeds schematically as follows:

$$\underset{(ZOH)}{\text{Acid site}} + \underset{(CH_3OH, CH_3OCH_3, \text{etc.})}{\text{methylating agent}} \rightarrow \underset{(ZOCH_3)}{\text{methylated acid site}} \quad \text{(i)}$$

$$\underset{(ZOCH_3)}{\text{methylated acid site}} \rightarrow \underset{(ZO^- \ldots CH_2)}{\text{surface stabilised carbene}} \quad \text{(ii)}$$

$$\underset{(ZO^- \ldots CH_2)}{\text{surface stabilised carbene}} \rightarrow \underset{(\text{e.g., } CH_2=CH_2)}{\text{first C–C bond}} \quad \text{(iii)}$$

Formation of the methylated acid site is the subject of the present section. The ongoing debate concerning the nature of the initial complex formed on methanol adsorption at an alumino–silicate Brønsted acid site [78–91] will not be discussed except to state that our current work suggests that at normal temperatures, the dominant adsorbed methanol species in acidic zeolites is a physisorbed species [91]. All reactions reported in the current work involving adsorbed methanol will be with respect to this physisorbed species.

A number of pathways for formation of a methylated acid site are conceivable. The simplest, a S_N2 reaction of a single CH_3OH molecule at a Brønsted acid site, [AlO(H)Si], has been studied by Blaskowskii and van Santen [85] and by Zicovich-Wilson et al. [92]. Due to different methodologies, the former reported an activation barrier of 184 kJ mol^{-1} whilst the latter reported a barrier of 217 or 171 kJ mol^{-1} depending on which oxygen site within their model cluster was methylated.

Another possibility for formation of the surface methoxyl species is that shown in Fig. 10, i.e., a pathway involving a single CH_3OH molecule but with more S_N1 character [91]. As expected on the basis of cluster calculations which omit long range electrostatic effects, no stable, charge separated S_N1 intermediate was observed. The calculated activation barrier for this process of around 230 kJ mol^{-1} at the TZVP/DFT(BLYP) level of theory indicates that this pathway is only likely to play a minor role in formation of the methylated acid site. We note however, that due to the polar nature of the mechanism, inclusion of long range electrostatic effects into the model is likely to lower the activation barrier.

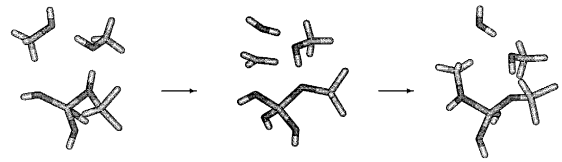

Fig. 11. HF/3-21G optimised structures for the methylation of a model Brønsted acid site by two methanol molecules. The acid site is modelled by a $(HO)_2AlO(H)SiH_3$ cluster and the central structure is the transition state.

A third possibility for the mechanism of reaction (i) is via interaction of two methanol molecules with the acidic Brønsted site, Fig. 11. We have been able to show that such a pathway proceeds with an activation barrier in the region of 130–160 kJ mol^{-1} at the MP2/6-31G**//HF/3-21G level of theory and using a range of model clusters [93]. The use of different model clusters also enabled us to demonstrate the significant effect of the difference in proton affinities of the two oxygen sites involved on the magnitude of the barrier. This effect was also discussed by Kramer et al. [2] who used it to rationalise the different reactivities of methane in MFI and faujasite type zeolites.

Finally, it is possible that dimethyl ether is the primary methylating agent in the initial stages of the MTG process. It is known that dimethyl ether forms almost immediately upon introduction of CH_3OH into acidic zeolites and well before the onset of hydrocarbon formation [94]. However, the literature is unclear as to whether dimethyl ether forms from the reaction of methanol with a surface bound methoxyl group ($ZOCH_3$) [95–97] or whether it forms from conventional condensation of methanol in

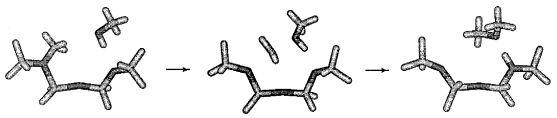

Fig. 12. HF/6-31G** optimised structures for formation of dimethyl ether from a methylated acid site and adsorbed methanol. The methylated acid site is modelled by a $H_3SiO(CH_3)Al(H)_2OSi(H)_2OSiH_3$ cluster and the central structure is the transition state.

the acidic environment of the zeolite pores [98,99].

HF/6-31G** calculations of the formation of $(CH_3)_2OH$ from CH_3OH and $ZOCH_3$ (Fig. 12) gave an activation barrier of 150 kJ mol^{-1} (desorption of the product was less activated). Assuming that the $ZOCH_3$ species was formed from adsorbed methanol (as above), the effective activation energy for formation of $(CH_3)_2OH^+$ (and from it, CH_3OCH_3) from methanol at a Brønsted acid site via a surface methoxyl species is estimated to be about 120 kJ mol^{-1}, i.e., the activation barrier of 150 kJ mol^{-1} plus the energy to form ZOMe (~ -5 kJ mol^{-1}) plus the energy of adsorption of CH_3OH at the methylated acid site (~ -25 kJ mol^{-1}). Estimates of the effect of electron correlation (at the MP2 level) suggest that the barrier should probably be lower at about 100 kJ mol^{-1}. This value compares with the gas phase activation barrier of ~ 35 kJ mol^{-1} for formation of $(CH_3)_2OH^+$ and H_2O from $CH_3OH_2^+$ and CH_3OH [100]. It is thus clear that CH_3OCH_3 probably forms from condensation of CH_3OH in the zeolite pores. CH_3OCH_3 is therefore a good candidate for the methylating agent responsible for formation of methylated acid sites. The reaction of CH_3OCH_3 at an alumino–silicate Brønsted acid sites is currently under study, with initial results suggesting that the activation barrier for formation of $ZOCH_3$ from adsorbed dimethyl ether is indeed lower than that for its formation from methanol. Further studies of this problem are reported in this volume by van Santen [6].

Although the mechanism of the MTG process is far from being understood, computational quantum chemistry methods are clearly bridging the gap in experimental knowledge.

3. Summary

The simulation studies described in this paper, together with those summarised in the other theoretical papers in this issue, clearly show the value of computational methods in modelling structure and reactivity in catalytic systems. With the rapid developments taking place in both computer hardware and software, these techniques are poised to play an even greater role in the development of a molecular understanding of catalysis.

Acknowledgements

We are grateful to Professor E.G. Derouane for the opportunity of presenting this work at the Franqui Colloquium held in his honour.

References

[1] C.R.A. Catlow (Ed.), Modelling of Structures and Reactivity in Zeolites (Academic Press, London, 1992).
[2] G.J. Kramer, R.A. van Santen, C.A. Emeis and A.K. Nowak, Nature 363 (1993) 529.
[3] J. Sauer, Stud. Surf. Sci. Catal. 84 (1994) 2039.
[4] C.R.A. Catlow, R.G. Bell and J.D. Gale, J. Mater. Chem. 4(6) (1994) 781.
[5] C.R.A. Catlow, R.G. Bell, J.D. Gale and D.W. Lewis, in: Zeolites: A Refined Tool for Designing Catalytic Sites, L. Bonneviot and S. Kaliaguina (Eds.) (Elsevier, Amsterdam, 1995), Stud. Surf. Sci. Catal. 97 (1995) 87.
[6] R.A. van Santen, these proceedings.
[7] K. Norskov, these proceedings.
[8] W.M. Meier, D.H. Olson and Ch. Baerlocher (Editors), Atlas of Zeolite Structure Types, 4th Ed., Elsevier, 1996.
[9] R.E. Morris, S.J. Weigel, N.J. Henson, L.M. Bull, M.T. Janicke, B.F. Chmelka and A.K. Cheetham, J. Am. Chem. Soc. 116 (1994) 11849.
[10] J.M. Bennett, J.P. Cohen, E.M. Flanigen, J.J. Pluth and J.V. Smith, in: Am. Chem. Soc. Symp. Ser., Vol. 218 (American Chemical Society, Washington, 1983) p. 109; S. Qiu, Q. Pang, H. Kessler and J.L. Guth, Zeolites 8 (1989) 440.

[11] A.R. Ruiz-Salvador, G. Sastre, D.W. Lewis and C.R.A. Catlow, J. Mater. Chem., (1996) in press.
[12] J.D. Gale and N.J. Henson, J. Chem. Soc. Faraday Trans. 90 (1994) 3175.
[13] M. Cole, A.N. Fitch, R. Goyal, R.H. Jones, A.J. Mora, H. Jobic and S.W. Carr, J. Mater. Chem. (1996), in press.
[14] A.J.M. de Man, W.P.J.H. Jacobs, J.P.W. Gilson and R.A. van Santen, Zeolites 12 (1992) 826.
[15] N.J. Henson, A.K. Cheetham and J.D. Gale, Chem. Mater. 8 (1996) 664.
[16] M.D. Shannon, J.L. Casci, P.A. Cox and S.J. Andrews, Nature 353 (1991) 417.
[17] P.A. Wright, S. Natarajan, J.M. Thomas, R.G. Bell, P.L. Gai-Boyes, R.H. Jones and J. Chen, Angew. Chem. Int. Ed. Engl. 31 (1992) 1472.
[18] M.A. Asensi, A. Corma and A. Martinez, J. Catal. 158 (1996) 561.
[19] P.R. Pujado, J.A. Rabo, G.J. Antos and S.A. Genbicki, Catal. Today 13 (1992) 113.
[20] D. Barthomeuf, in: Acidity and Basicity in Solids. Theory, Assessment and Utility, Vol. 444, J. Fraissard, L. Petrakis (Eds.), NATO ASI Series C (1993) p. 375.
[21] G. Sastre, D.W. Lewis and C.R.A. Catlow, J. Phys. Chem. 100 (1996) 6722.
[22] M. Briend, D. Barthomeuf, in: Proc. of the 9th Int. Zeolite Conf., von R. Ballmoos, J.B. Higgins and M.M.J. Treacy (Eds.) (Butterworth-Heinemann, Boston, 1993) p. 635.
[23] A.F. Ojo, J. Dwyer, J. Dewing, P.J. O'Malley and A. Nabhan, J. Chem. Soc. Faraday Trans. 88 (1992) 105.
[24] D. Barthomeuf, Zeolites 14 (1994) 394.
[25] E.M. Flanigen, R.L. Patton and S.T. Wilson, in: Innovation in Zeolite Material Science, Grobet, P.J. et al. (Eds.), Stud. Surf. Sci. Catal. 37 (1988) 13.
[26] R. Burch, Catal. Today 26 (1995) 97.
[27] M. Iwamoto, H. Yahiro, N. Mizuno, W.-X. Zhang, Y. Mine, H. Furukawa and S. Kagawa, J. Phys. Chem. 96 (1992) 9360.
[28] J.D. Gale, GULP, General Utility Lattice Programme (Royal Institution of Great Britain and Imperial College, London, 1992–1996).
[29] D.H. Gay and A.L. Rohl, J. Chem. Soc. Faraday Trans. 91(5) (1995) 925.
[30] N.L. Allan, A.L. Rohl, D.H. Gay, C.R.A. Catlow, R.J. Davey and W.C. Mackrodt, Faraday Discuss. 95 (1993) 273.
[31] A.L. Rohl, D.H. Gay, R.J. Davey and C.R.A. Catlow, J. Am. Chem. Soc. 118 (1996) 642.
[32] A.R. George, K.D.M. Harris, A.L. Rhol and D.H. Gay, J. Mater. Chem. 5(1) (1995) 133–139.
[33] M.A. Nygren et al., to be published.
[34] C.M. Freeman, C.R.A. Catlow, J.M. Thomas and S. Brode, Chem. Phys. Lett. 186 (1991) 137.
[35] R.G. Bell, D.W. Lewis, P. Voigt, C.M. Freeman, J.M. Thomas and C.R.A. Catlow, Stud. Surf. Sci. Catal. 84 (1994) 2075.
[36] A.A. Shubin, C.R.A. Catlow, J.M. Thomas and K.I. Zamaraev, Proc. R. Soc. Lond. A 446 (1994) 411.
[37] D.W. Lewis, C.M. Freeman and C.R.A. Catlow, J. Phys. Chem. 99 (1995) 11194.
[38] A.P. Stevens and P.A. Cox, J. Chem. Soc. Chem. Commun. (1995) 343.
[39] S.J. Weigel, J.C. Gabriel, E.G. Puebla, A.M. Bravo, N.J. Henson, L.M. Bull. and A.K. Cheetham, J. Am. Chem. Soc. 118 (1996) 2427.
[40] Z.A. Kaszkur, R.H. Jones, D. Waller, C.R.A. Catlow and J.M. Thomas, J. Phys. Chem. 97 (1993) 426.
[41] Z.A. Kaszkur, R.H. Jones, R.G. Bell, C.R.A. Catlow and J.M. Thomas, Mol. Phys. (1996), in press.
[42] C.M. Freeman, D.W. Lewis, T.V. Harris, A.K. Cheetham, N.J. Henson, P.A. Cox, A.M. Gorman, S.M. Levine, J.M. Newsam, E. Hernandez and C.R.A. Catlow, in: Computer-Aided Molecular Design. Applications in Agrochemicals, Materials and Pharmaceuticals, C.H. Reynolds, M.K. Holloway and H.K. Cox (Eds.) (American Chemical Soc., Washington D.C., 1995) p. 326.
[43] P.A. Cox, A.P. Stevens, L. Banting and A.M. Gorman, in: Zeolites and Related Microporous Materials: State of the Art 1994. Proc. of the 10th Int. Zeolite Assoc. Meet., J. Weitkamp, H.G. Karge, H. Pfeifer and W. Holderich (Eds.), Vol. 84 (Elsevier, Amsterdam, 1994) Stud. Surf. Sci. Catal., p. 2115.
[44] T.V. Harris and S.I. Zones, in: Zeolites and Related Microporous Materials: State of the Art 1994. Proc. of the 10th Int. Zeolite Assoc. Meet., J. Weitkamp, H.G. Karge, H. Pfeifer and W. Holderich (Eds.), Vol. 84 (Elsevier, Amsterdam, 1994), Stud. Surf. Sci. Catal., p. 29.
[45] H. Gies and B. Marler, Zeolites 12 (1992) 42.
[46] S.L. Burkett and M.E. Davis, Chem. Mater. 7 (1995) 920, 1453; J. Phys. Chem. 98 (1994) 4647.
[47] D.W. Lewis, C.R.A. Catlow and J.M. Thomas, Chem. Mater. 8 (1996) 1112.
[48] C. Urbina de Navarro, F. Machado, M. Lopez, M. Maspero and J. Perez-Pariente, Zeolites 15 (1995) 157.
[49] M.G. Uytterhoeven and R.A. Schoonheydt, Microporous Mater. 3 (1994) 265.
[50] B. Kraushaar-Czarnetzki, Q.G.M. Hoogervorst, R.R. Andrea, C.A. Emeis and W.H.J. Stork, J. Chem. Soc. Faraday Trans. 87 (1991) 891.
[51] G.J. Hutchings, M.S. Scurrell and J.R Woodhouse, Chem. Soc. Rev. 18 (1989) 251.
[52] J.H. Lunsford, Angew. Chem. Int. Ed. Engl. 34 (1995) 970.
[53] S.P. Mehandru, A.B. Anderson and J.F. Brazdil, J. Am. Chem. Soc. 110 (1988) 1715.
[54] C.M. Zicovich-Wilson, R. González-Luque and P.M. Viruela-Martín, J. Mol. Struct. (THEOCHEM) 208 (1990) 153.
[55] P.M. Viruela-Martín, R. Viruela-Martín, C.M. Zicovich-Wilson and F. Tomás-Vert, J. Mol. Catal. 64 (1991) 191.
[56] K.J. Børve and L.G.M. Pettersson, J. Phys. Chem. 95 (1991) 3214.
[57] K.J. Børve and L.G.M. Pettersson, J. Phys. Chem. 95 (1991) 7401.
[58] K.J. Børve, J. Chem. Phys. 95 (1991) 4626.
[59] J.L. Anchell, K. Morokuma and A.C. Hess, J. Chem. Phys. 99 (1993) 6004.

[60] K.D. Campbell, E. Morales and J.H. Lunsford, J. Am. Chem. Soc. 109 (1987) 7900.
[61] Y. Feng and D. Gutman, J. Phys. Chem. 95 (1991) 6556; Y. Feng, J. Niiranen, D. Gutman, J. Phys. Chem. 95 (1991) 6564.
[62] H.S. Zhang, J.X. Wang, D.J. Driscoll and J.H. Lunsford, J. Catal. 112 (1988) 366.
[63] C.H. Lin, J.X. Wang and J.H. Lunsford, J. Catal. 111 (1988) 302.
[64] D.J. Driscoll, W. Martir, J.X. Wang and J.H. Lunsford, J. Am. Chem. Soc. 107 (1985) 58.
[65] E.G. Derouane, J.G. Fripiat and J.M. André, Chem. Phys. Lett. 28 (1974) 445.
[66] S.A. Pope, M.F. Guest, I.H. Hillier, E.A. Colbourn, W.C. Mackrodt and J. Kendrick, Phys. Rev. B 28 (1983) 2191.
[67] H. Kobayashi, D.R. Salahub and T. Ito, J. Phys. Chem. 98 (1994) 5487.
[68] G.M. Zhidomirov, V.I. Avdeev, N.U. Zhanpeisov, I.I. Zakharov and I.Y. Yudanov, Catal. Today 24 (1995) 383.
[69] R. Orlando, F. Corà, R. Millini, G. Perego and R. Dovesi, submitted for publication.
[70] C.R.A. Catlow, R.A. Jackson and J.M. Thomas, J. Phys. Chem. 94 (1990) 7889.
[71] L. Ackermann, J.D. Gale and C.R.A. Catlow, to be published.
[72] A.D. Becke, Phys. Rev. A38 (1988) 3098.
[73] C. Lee, W. Yang and R.G. Parr, Phys. Rev. B 37 (1988) 786.
[74] T. Ziegler, Chem. Rev. 91 (1991) 651.
[75] P. Politzer, J.M. Seminario (Eds.), Density Functional Theory: A Tool for Chemistry (Elsevier, 1995).
[76] S.L. Meisel, J.P. McCullogh, C.H. Lechthaler and P.B. Weisz, Chemtech 6 (1976) 86.
[77] G.J. Hutchings and R. Hunter, Catal. Today 6 (1990) 279.
[78] R. Vetrivel, C.R.A. Catlow and E.A. Colbourn, J. Phys. Chem 89 (1989) 4594.
[79] J.D. Gale, C.R.A. Catlow and A.K. Cheetham, J. Chem. Soc. Chem. Commun. (1991) 178.
[80] J. Sauer, C. Kölmel, F. Haase and R. Ahlrichs, Proc. 9th Int Zeo. Conf, Montreal (1992) p. 679.
[81] J.D. Gale, C.R.A. Catlow and J.R. Carruthers, Chem. Phys. Lett. 216 (1993) 155.
[82] F. Haase and J. Sauer, J. Phys. Chem. 98 (1994) 3083.
[83] S. Bates and J. Dwyer, J. Mol. Struct. (Theochem) 306 (1994) 57.
[84] F. Haase and J. Sauer, J. Am. Chem. Soc. 117 (1995) 3780.
[85] S.R. Blaskowskii and R.A. van Santen, J. Phys. Chem. 99 (1995) 11728.
[86] S.P. Greatbanks, Ph.D. thesis, University of Manchester (1995), submitted.
[87] J.D. Gale, in: Topics in Catalysis, Special Issue 'Recent Advances in the Study and Preparation of Novel Surfaces, C.R.A. Catlow and J.M. Thomas (Eds.), Vol. 3 (1996) pp. 1–2.
[88] R. Shah, M.C. Payne, M.-H. Lee and J.D. Gale, Science 271 (1996) 1395.
[89] J. Limtrakul, Chem. Phys. 193 (1995) 79.
[90] E. Nusterer, P.E. Blöchl and K. Shwarz, Angew. Chem. Int. Ed. Engl. 35 (1996) 175.
[91] P.E. Sinclair and C.R.A. Catlow, manuscript in preparation.
[92] C.M. Zicovich-Wilson, P. Viruela and A. Corma, J. Phys. Chem. 99 (1995) 13224.
[93] P.E. Sinclair and C.R.A. Catlow, J. Chem. Soc. Faraday Trans. 92(12) (1996) 2099–2105.
[94] C.D. Changs and A.J. Silvestri, J. Catal 47 (1977) 249.
[95] L. Kubelkova, J. Novakova and K. Nedomova, J. Catal. 124 (1991) 441.
[96] J. Bandiera and C. Naccache, Appl. Catal. 97 (1991) 10732.
[97] C.E. Bronnimann and G.E. Maciel, J. Am. Chem. Soc. 108 (1986) 7154.
[98] C. Tsiao, D.R. Corbin and C. Dybowski, J. Am. Chem. Soc. 112 (1990) 7140.
[99] M.W. Anderson and J. Klinowski, J. Am. Chem. Soc. 112 (1990) 10.
[100] E.P. Grimsrud and P. Kebarle, J. Am. Chem. Soc. 95 (1973) 7939.